Results in Engineering 29 (2026) 109560

Contents lists available at ScienceDirect

Results in Engineering

journal homepage: www.sciencedirect.com/journal/results-in-engineering

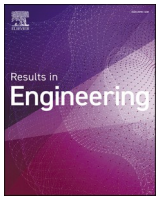

Research paper

Multifunctionality of quinoxaline derivatives with variable room temperature phosphorescence for luminescent tags, morphological imaging, single-emitter white OLEDs, and highly sensitive oxygen sensors

Mohamed Abdella [a], Matas Guzauskas [a], Jurate Simokaitiene [a], Asta Dabuliene [a], Monika Cekaviciute [a], Dmytro Volyniuk [a], Vitaly E. Matulis [b], Ekaterina G. Ragoyja [b], Juozas V. Grazulevicius [a,*]

[a] Department of Polymer Chemistry and Technology, Kaunas University of Technology, K. Barsausko st.59, LT- 51423, Kaunas, Lithuania
[b] Computer, Electrical and Mathematical Science and Engineering Division, 4700 King Abdullah University of Science and Technology, Thuwal 23955-6900, Saudi Arabia

ARTICLE INFO

Keywords:
Quinoxaline
Room temperature phosphorescence
Oxygen sensor
Luminescent tag
Single-emitter white organic light-emitting diode

ABSTRACT

The impact of room temperature phosphorescence (RTP) of the derivatives of quinoxaline derivatives on their multifunctional properties is investigated for the estimation of applicability in luminescent tags, morphological imaging, single-emitter white organic light-emitting diodes (OLEDs), and oxygen sensors. The differences in the phosphorescence spectra of the compounds are attributed to their electronic structure. The molecular dispersions in the rigid polymer matrix of the quinoxaline derivatives with either rigid or flexible molecular structures, with or without bromine atoms, show green to orange RTP with quantum yields of up to 45.6 % and RTP lifetimes from 0.83 to 525 ms. The extremely high ratio of RTP to fluorescence quantum yields, reaching 910, is observed for the molecular mixtures of the quinoxaline derivatives with the polymeric host. This property enables the use of quinoxaline derivatives as the state-of-the-art active materials for luminescence tags or morphological imaging. OLEDs with the emitting layers of the quinoxaline derivatives molecularly dispersed in a charge-transporting host, exhibit the combination of blue fluorescence and orange RTP resulting in white electroluminescence with CIE1931 coordinates (x, y) ranging from (0.32–0.41, 0.31–0.45) and colour rendering indexes between 71 and 83. Due to efficient RTP, the studied quinoxaline derivatives are ideally suited for oxygen sensors. The high oxygen sensitivity of one synthesized RTP emitter with the emission lifetime of 525 ms enables to reach the Stern-Volmer constants of up to 1.1×10^{-3} ppm^{-1} which is among the highest ones reported up to now.

1. Introduction

Efficient phosphorescence of the iridium complex allowed to reach internal quantum efficiency (IQE) of 68.5 % and external quantum efficiency (EQE) of 13.7% of organic light-emitting devices (OLEDs) back in 1999 [1]. Since then, despite the growing costs and environmental issues, the noble metals containing phosphorescent complexes have become the most important emitters of OLEDs used in modern, lightweight, flexible, slim, transparent displays and in lightning devices [2]. Many noble metal-free organic emitters exhibiting thermally activated delayed fluorescence (TADF) were developed for single-colour OLEDs showing perfect emission colour purity and high EQEs [3]. Deep-blue hyperfluorescent OLEDs with EQE of 41.3% with organic emitters displaying multiresonance-induced TADF were recently reported [4]. In contrast to the single-colour emitters, the development of white-emitting organic compounds is still in the initial stage [5]. The single-emitter white OLEDs still show very low efficiencies and pure stability of white electroluminescence under the different voltages. For example, single-emitter white OLEDs with maximum EQE of 6.2% and relatively pure emission colour stability were recently developed using white emitting iridium complex [6]. Noble metal-free single molecular white OLEDs based on a mechanochromic TADF emitter demonstrated maximum EQE of 0.49 % and white electroluminescence only at a narrow range of applied voltages [7]. Single molecular white emission

* Corresponding author.
E-mail address: juozas.grazulevicius@ktu.lt (J.V. Grazulevicius).

https://doi.org/10.1016/j.rineng.2026.109560
Received 7 July 2025; Received in revised form 3 February 2026; Accepted 11 February 2026
Available online 11 February 2026

can be obtained for noble metal-free RTP materials when the appropriate combination of fluorescence and RTP is achieved [8–10]. We obtained such a combination for thianthrene-based luminophores exhibiting single-molecular white emission with high photoluminescence quantum yields of 84 % due to the balance between intersystem crossing and the relaxation of the singlet excitons [11]. These derivatives were not used for the development of RTP OLEDs because of the low glass transition temperatures. The aim of this study partly hints at fully organic RTP emitters for white OLEDs with the single molecular emitter. In addition, the advantages of the RTP materials make them potential candidates for the applications in the fields of photonics and optoelectronics, including sensing, electroluminescent devices, anticounterfeiting, memorising, bioimaging, microfluidic visualisation, X-ray detection or even quantum computing [12–14]. RTP is typically detectable in the environments devoid of oxygen, as oxygen has the capability to suppress excited triplet states [15–19].

Excited triplet states of organic molecules intrinsically have lengthy lifetimes and consequently undergo dissipation through molecular vibrations and rotations (i.e., thermal deactivation) because of the participation of spin-forbidden transitions (i.e., S_1 to T_1; T_1 to S_0) [20,21]. The contribution of heavy metals, are usually employed to stabilize the emission by large spin-orbit couplings

(SOCs) [22]. Organic luminophores exhibiting RTP are appealing replacements for organic metal complexes due to their relatively low cost, environmental friendliness, flexible synthesis and stability [23]. In the last ten years, there have been notable progress in the development of new materials that demonstrate enduring and consistent RTP which is achieved through the understanding and control of the process [24,25]. For example, colourful afterglow displays were proposed using indolinone-based triplet emitters exhibiting cyan to yellow phosphorescence with the long lifetime of 700 ms and unknown RTP quantum yields [26]. The derivative of 9,9-dimethylacridine and naphthalimide with RTP quantum yield of 6.1 % and the lifetime of 210 ms showed promising results as the components of anti-counterfeiting labels [27]. Multifunctional crystalline blue RTP emitters with emission quantum yields of up to 96.5% and RTP lifetimes varying from 101.2 to 199.17 ms were used for data encryption, fingerprint identification and afterglow display under ambient conditions [28]. 4-(Allyloxy)-4′-bromo-1, 1′-biphenyl derivatives were used for the development of X-ray responsive amorphous copolymers showing efficient RTP with quantum yields of up to 51.4% and RTP lifetimes varying from 9.22 to 11.76 ms [29]. Programmable luminescent tags were developed using natural organic triplet emitters such as quinoline alkaloids derivatives of quinine, quinidine, cinchonine, cin-chonidine[30]. They showed high ratio of RTP to fluorescence quantum yields (P2F) ranging from 0.7 to 9.1 [30]. We recently developed very oxygen-sensitive probes, i.e. a derivative of phenothiazine and triazatriazatruxene [31]. Its molecular dispersion in the rigid polymer matrix showed RTP with the quantum yield of 54%, RTP lifetime of 16.6 ms and P2F of 18 [31]. The ultralong RTP lifetime of 5.92 s was observed for dibenzo[f,h]quinoxaline-based polymers applicable for fingerprint identification and multiple information encryption [32]. Multicolour RTP compounds containing rigid moieties were proposed for 3D-printing [33]. Thus, different RTP emitters were proposed for specific photonic or optoelectronic applications. However, the multifunctional RTP compounds are somewhat rare. To reveal the potential of quinoxaline derivatives as multifunctional RTP emitters, we synthesized four compounds with yields above 70%. We also studied their RTP properties keeping in mind the different possible applications. The compounds exhibit very efficient RTP. It was observed for solutions, neat films, and for the films of their molecular mixtures with charge-transporting or polymeric hosts. OLEDs based on these compounds showed white electroluminescence with high colour quality corresponding to CIE1931 coordinates (x, y) of (0.32–0.41, 0.31–0.45) and a colour rendering index of 83. When molecularly dispersed in a polymeric host, the studied derivatives of quinoxaline showed P2R of up to 910. This observation shows that the compounds are suitable for oxygen sensing, emissive tags and imaging.

2. Results and discussion

2.1. Synthesis

Scheme 1 shows the pathway for the synthesis of four quinoxaline derivatives (DPQ, BrDPQ, AcNQ, and BrAcNQ). The synthesis includes condensation reactions between benzil or acenaphthenequinone and 3,6-dibromobenzene-1,2-diamine or o-phenylenediamine. These reactions produce the target compounds with the yields above 70%. The synthesis of DPQ and AcNQ was reported earlier [34,35].

The detailed description of the synthesis of the compounds and the data of their characterization are given in the supporting information (Figs. S1-S12).

2.2. Theoretical calculations

The geometry and electronic structure of compounds DPQ, BrDPQ, AcNQ, and BrAcNQ in ground and excited states were investigated in toluene solution within density functional theory (DFT) using MN15 functional [36] with 6-31+G(d) basis set. According to the literature [37], this level of theory provides good agreement with experiment when calculating the optical properties of organic compounds. Solvation effects were considered using the SMD model [38] in terms of Linear Response scheme [39]. For the calculations of the absorption spectra the geometries of the ground states (S_0) of the compounds were fully optimized in solution within DFT approach with subsequent calculation of the spectra within TD-DFT. For the calculations of emission spectra, the geometries of singlet and triplet excited states were fully optimized in solution within TD-DFT. All the calculations were carried out using Gaussian16 program [40]. The analysis of electron density was performed using Multiwfn software [41].

The calculated absorption spectra of the compounds are compared with experimental data obtained for toluene solutions (Fig. 1). The calculated spectra agree well with the experimental data within the systematic error (blue shift) typical for TD-DFT. Table 1 provides computational data for absorption wavelengths (λ_{ABS}), oscillator strengths (f), separation degree of positive (ρ_+) and negative (ρ_-) parts of electron density (τ-indexes) and overlaps between functions C_+ and C_- [41], S_{+-}-indexes corresponding to the lowest energy excitations of the studied compounds. The calculated plots of natural transition orbitals (NTOs) for $S_0 \rightarrow S_n$ transitions are presented in Fig. 3.

According to the calculational data, the $S_0 \rightarrow S_1$ transitions for both DPQ and BrDPQ correspond to n-π* excitations (Fig. 2). As a result, these transitions exhibit low oscillator strengths and are not visible in the absorption spectra. In contrast, the $S_0 \rightarrow S_2$ transitions that are responsible for the absorption maxima in the experimental spectra of DPQ and BrDPQ correspond to π-π* excitations in which HOMO and LUMO are involved. Additionally, both of the compounds exhibit another absorption peaks ($\lambda_{ABS} < 300$ nm, not fully captured in the experimental spectra in Fig. 1) corresponding to $S_0 \rightarrow S_5$ transitions, that also arise from π-π* excitations in which HOMO and LUMO+1 are involved. The calculated values of the largest coefficients in the CI expansion are provided in Table S3.

For AcNQ and BrAcNQ, a slightly different pattern is observed. Absorption maxima in the experimental spectra correspond to $S_0 \rightarrow S_3$ and $S_0 \rightarrow S_5$ transitions (Table 1) that are π-π* excitations (Fig. 3). The $S_0 \rightarrow S_1$ transitions in both structures are characterized by low oscillator strength due to their n-π* nature. In contrast, the $S_0 \rightarrow S_2$ and $S_0 \rightarrow S_4$ transitions involve π-π* excitations but are also characterized by relatively low oscillator strengths. Analysis of the NTO plots (Fig. 3) provides a compelling explanation of this observation. The HONTO and LUNTO distributions for $S_0 \rightarrow S_2$ and $S_0 \rightarrow S_4$ transitions reveal an alternating pattern of electron density, where electron-deficient and electron-rich regions interchange between HONTO and LUNTO. The similar

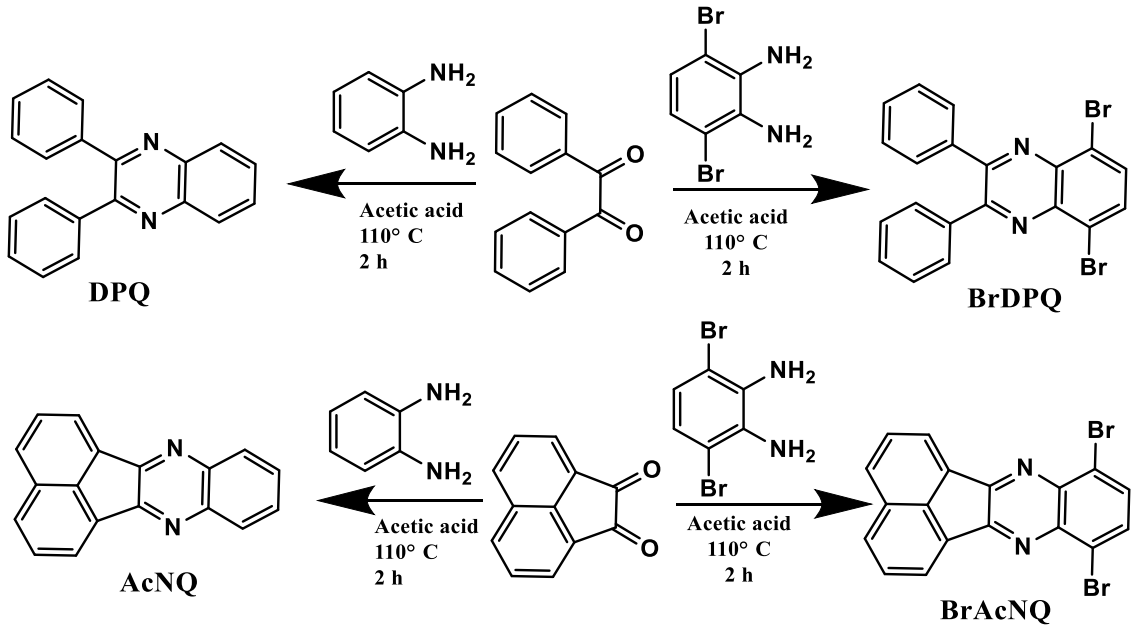

Scheme 1. Synthetic route for compounds DPQ, BrDPQ, AcNQ, and BrAcNQ.

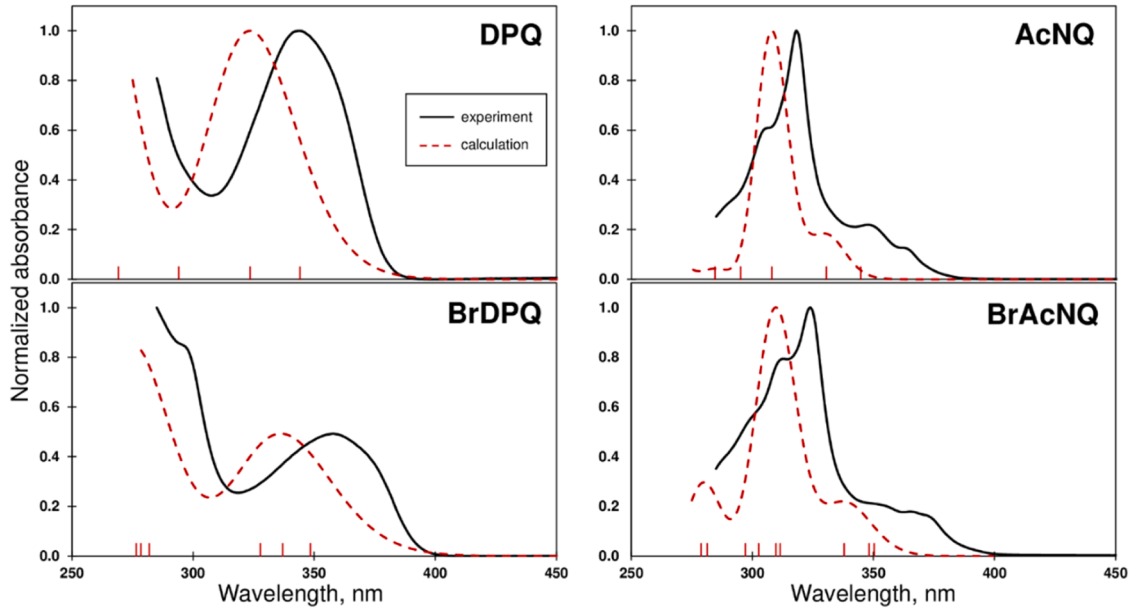

Fig. 1. MN15/6-31+G(d) calculated and experimental absorption spectra of toluene solutions of DPQ, AcNQ, BrDPQ, and BrAcNQ. Calculated wavelength values corresponding to $S_0 \rightarrow S_n$ transitions are marked with red dashes.

electronic delocalization effect is observed in multi-resonant TADF (MR-TADF) systems [42], which typically contain rigid planar π-conjugated frameworks with electron-donating and electron-withdrawing heteroatoms. In AcNQ and BrAcNQ, the similar but weaker effects are achieved without electron-withdrawing heteroatoms. The possibility of design of multi-resonant systems without acceptor fragments has been previously shown in the literature [42]. In the work mentioned, the corresponding transitions with short-range charge transfer (SRCT) also showed low oscillator strengths and weak absorption bands in solution. The calculated values of τ- and S_{+-}-indexes (Table 1) also confirm that none of the studied $S_0 \rightarrow S_N$ transitions for compounds AcNQ and BrAcNQ exhibit long-range charge transfer.

Based on comparison of pairs DPQ–BrDPQ and AcNQ–BrAcNQ we can derive that the introduction of Br atom (a substituent with strong –I and weak +M effects) in the molecules leads to red shift of the absorption maxima. This observation is explained by the fact that the transitions responsible for the absorption maxima in the spectra involve π-π* excitations. Consequently, the bromine atom affects orbital energies primarily through its donor +M effect. This results in increase of the HOMO energy. Therefore, the excitation energy decreases, which leads to the increase in the absorption wavelength (red shift).

The calculated data shows that fluorescence maxima for all the structures correspond to $S_1 \rightarrow S_0$ transition. In case of phosphorescence, $T_1 \rightarrow S_0$ (DPQ and BrDPQ) or $T_1 \rightarrow S_0$ and $T_2 \rightarrow S_0$ (AcNQ and BrAcNQ) transitions are manifested in the experimental emission spectra. The calculated fluorescence wavelength values are in rather good agreement with the experimental ones (Tables 2 and 5). Systematic error (blue shift) is close to that obtained by the calculations of absorption spectra

Table 1
MN15/6-31+G(d) calculated values of absorption wavelengths (ABS), oscillator strengths (f), τ- and S+–indexes for the lowest energy excitations of DPQ, AcNQ, BrDPQ, and BrAcNQ.

Transition		$S_0 \rightarrow S_1$	$S_0 \rightarrow S_2$	$S_0 \rightarrow S_3$	$S_0 \rightarrow S_4$	$S_0 \rightarrow S_5$
DPQ	λ_{ABS}, nm	344	323 (344)[a]	294	269	266
	f	0.0029	0.4924	0.0043	0.0322	0.3395
	τ-index	–1.720	–0.434	–1.178	–1.820	–1.961
	S_{+-}	0.8922	0.9063	0.956	0.9069	0.9819
BrDPQ	λ_{ABS}, nm	348	337 (358)[a]	328	282	278
	f	0.0074	0.4378	0.0446	0.1208	0.4022
	τ-index	–1.964	–0.176	–0.712	–1.808	–0.529
	S_{+-}	0.9311	0.8872	0.9177	0.9596	0.8949
AcNQ	λ_{ABS}, nm	345	331	331 (349)[a]	309	308 (318)[a]
	f	0.0027	0.0007	0.2172	0.0013	1.2232
	τ-index	–1.804	–1.715	–1.834	–1.812	–2.391
	S_{+-}	0.8779	0.9844	0.9795	0.9687	0.9710
BrAcNQ	λ_{ABS}, nm	350	348	338 (352)[a]	311	310 (324)[a]
	f	0.0020	0.0264	0.2422	0.0125	1.1783
	τ-index	–1.885	–2.067	–1.620	–1.240	–2.048
	S_{+-}	0.8954	0.969	0.9749	0.9575	0.9852

a The experimental values of ABS are given in brackets.

(Table 1). For all the calculated phosphorescence maxima significant red shift with respect to experimental wavelengths is observed. Nevertheless, such deviation is rather natural because of well-known tendency of DFT methods to lower energies of triplet electronic states. It is of great importance that qualitative positions of phosphorescence maxima of the studied structures are consistent with the experimental ones.

For room-temperature phosphorescence (RTP) to occur, efficient intersystem crossing (ISC) from photoexcited singlet states to triplet states must take place. To study the possibility of such conversion, spin-orbit coupling (SOC) values for $S_n \rightarrow T_n$ (n=0–15) were calculated. The calculations were performed on the basis of TD-DFT results using PySOC program [43]. NTO plots for $S_0 \rightarrow T_n$ transitions of the studied structures are shown in Fig. 4. More details on MOs plots and energies can be found in Supporting Information (Tables S2, S15–S18).

From the point of view of possibility of conversion into triplets, the most promising are singlet excited states (S_N) which are characterized by low oscillator strength for $S_0 \rightarrow S_n$ transition and, consequently, longer lifetime. Thus, for all of the structures S_1 excited states are the most interesting from the point of view of ISC. It is also known that ISC rate depends both on SOC value and energy gap between corresponding excited states. Therefore, the SOC values only for the lowest-energy triplet excited states are presented in Table 3.

In case of DPQ and BrDPQ $S_1 \rightarrow T_1$ conversion seems to be likely. These excited states are characterized by large SOC values and have smaller energy gap than the other pairs with the large SOC values ($S_3 – T_3$ for DPQ; $S_3 – T_3$ and $S_4 – T_1$ for BrDPQ). This suggests that efficient $S_1 \rightarrow T_1$ conversion followed by $T_1 \rightarrow S_0$ phosphorescence is feasible for DPQ and BrDPQ. High S_1–T_1 SOC values are consistent with qualitative El-Sayed rule: $S_0 \rightarrow S_1$ and $S_0 \rightarrow T_1$ transitions have different nature (n-π* and π-π* correspondingly).The other conversion paths are also possible ($S_3 – T_3$). Nevertheless, they also lead to $T_1 \rightarrow S_0$ phosphorescence in agreement with the Kasha rule. Thus, the ISC to higher triplet excited states does not lead to multiple phosphorescence maxima because of the efficient nonradiative $T_n \rightarrow T_1$ transitions.

In contrast, for symmetric planar compounds AcNQ and BrAcNQ the $S_1 \rightarrow T_1$ ISC path is unlikely because of very small SOC values. For these structures S_1 and T_2 states are characterized by large SOC values which suggests efficient $S_1 \rightarrow T_2$ conversion. Similarly, to DPQ and BrDPQ, conversion to higher triplet states is also possible.

It is important to note, that differences in structures and symmetries of DPQ, BrDPQ and AcNQ, BrAcNQ leads to striking difference in phosphorescence nature. The rigid planar structures (AcNQ and BrACNQ) possess small SOC values for $S_0 – T_1$ and large values for $S_0 – T_2$ which leads to the impeded conversion from T_2 to T_1. Consequently, for

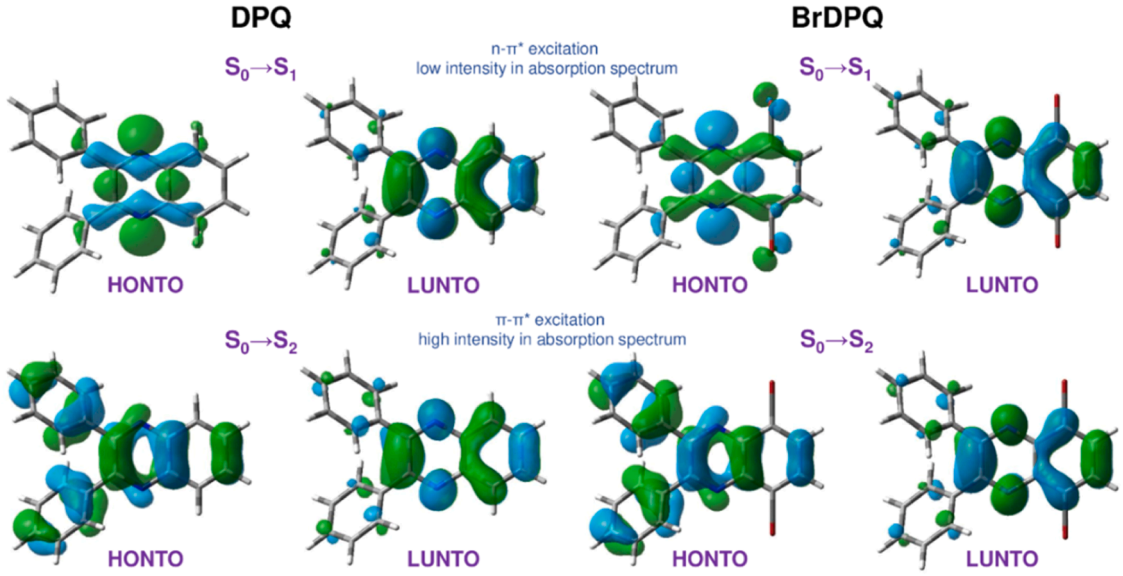

Fig. 2. Calculated plots of $S_0 \rightarrow S_n$ NTOs of DPQ and BrDPQ (n=1–2).

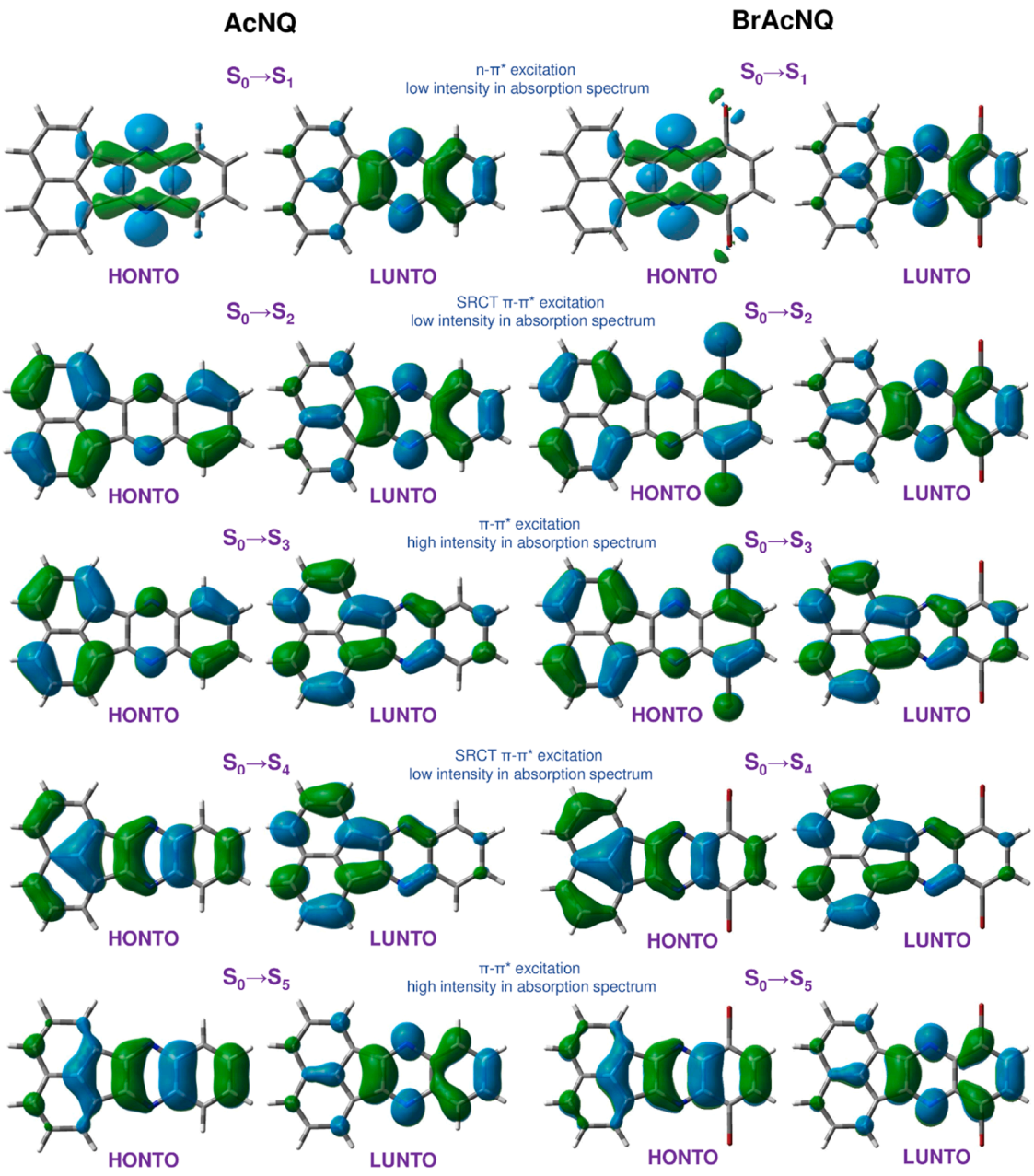

Fig. 3. Calculated plots of $S_0 \rightarrow S_n$ NTOs of AcNQ and BrAcNQ (n=1–5).

Table 2
MN15/6-31+G(d) calculated wavelengths corresponding to fluorescence (FL) and phosphorescence (PH) maxima of the studied compounds.

	DPQ	BrDPQ	AcNQ	BrAcNQ
λ_{FL}, nm	406	403	412	407
λ_{PH}, nm	654	738	708, 607	703, 689

such structures the non-Kasha emission from T_2 becomes possible, leading to the dual phosphorescence ($T_2 \rightarrow S_0$ and $T_1 \rightarrow S_0$) observed experimentally in case of AcNQ and BrAcNQ. These findings are consistent with the results of work [44] in which similar non-Kasha emission was predicted for rigid planar quinoxaline derivatives.

2.3. Thermal analysis

Differential scanning calorimetry (DSC) measurements and thermogravimetric analysis (TGA) were conducted for the estimation of the character and the temperatures of the morphological transitions and of the temperatures and the reasons of the initial weight losses. The results of the DSC measurements show that the powders of the synthesized compounds possess the crystalline structures. When crystals of organic compounds experience the decrease of the freedom of molecular movements and when oxygen penetration is prevented, efficient RTP can occur even in air [28,45]. The crystallization temperatures (T_{cr}) of 226°C is observed for compound BrAcNQ (Table 4). BrAcNQ also exhibits the highest melting point at 301°C. The highest T_{cr} and T_m values of BrAcNQ suggest compact packing of molecules in crystals. This can be caused by the planar molecular structure of the compound. The lower T_{cr} and T_m values of DPQ, BrDPQ, AcNQ can apparently be attributed to the decreased planarity of the molecules. The higher T_{cr} and T_m of AcNQ and BrAcNQ relative to those of DPQ and BrDPQ indicate that their molecules are more tightly packed in the crystalline phase. Two melting temperatures were detected for DPQ during the initial DSC heating scan

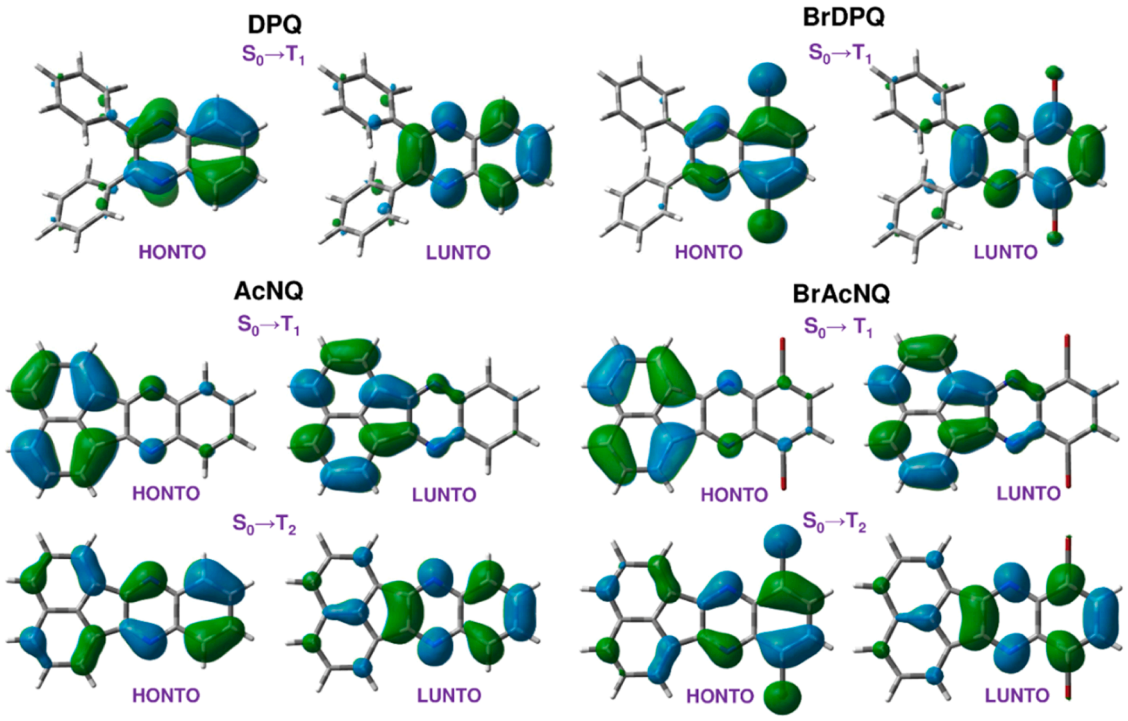

Fig. 4. Calculated plots of $S_0 \rightarrow T_n$ NTOs of DPQ, BrDPQ (n=1) and AcNQ, BrAcNQ (n=1–2).

Table 3
Calculated spin-orbit coupling values for $S_n \rightarrow T_n$ transitions of the studied compounds.

Electronic states	SOC, cm^{-1} (root-sum-square values)			
	DPQ	BrDPQ	AcNQ	BrAcNQ
S_0–T_1	0.6547	4.7214	0.0000	0.0000
S_0–T_2	4.6527	5.9236	0.2073	0.5696
S_0–T_3	1.0203	20.2708	0.0410	22.3677
S_1–T_1	8.5602	48.7326	0.0429	4.0370
S_1–T_2	1.6071	8.2809	9.1763	41.5657
S_1–T_3	2.6317	33.2710	0.0000	0.0000
S_2–T_1	1.0810	24.8850	0.2232	0.2262
S_2–T_2	0.4132	0.2389	0.0000	0.0000
S_2–T_3	1.8153	18.7740	6.7306	51.7796
S_3–T_1	2.0880	24.2368	0.0000	0.0000
S_3–T_2	0.4992	23.2254	0.6776	0.3025
S_3–T_3	7.4909	84.9898	0.2868	7.9057
S_4–T_1	1.0296	71.3287	0.0925	0.2998
S_4–T_2	2.9180	0.8785	0.0000	0.0000
S_4–T_3	0.9027	40.2315	4.6849	50.2832
S_5–T_1	0.3811	5.2767	0.0000	0.0000
S_5–T_2	0.9872	7.5802	0.6261	0.1429
S_5–T_3	1.6521	36.9679	0.3442	12.1881

Table 4
The temperatures of decomposition and the phase transitions of DPQ, AcNQ, BrDPQ, and BrAcNQ.

Compound	$T_{-5\%}$ (°C)	T_m (°C)	T_{cr} (°C)	T_g (°C)
DPQ	233	123, 128	88	22
AcNQ	248	241	207	-
BrDPQ	252	222	144	-
BrAcNQ	285	301	266	-

(Fig. S13). This observation is attributed to polymorphism of DPQ. The ability of glass formation was observed only for DPQ. The glass transition temperature (T_g) of 22°C was observed in the second DSC heating scan (Figs. 5b, S13, Table 4). Taking into account the low T_g of DPQ, the hosts with high T_g (e.g. Zeonex (T_g of 162°C) [46] or TCTA (T_g of 151°C) [47]) have to be used for the estimation of its applicability in the devices.

Fig. 5a shows TGA curves of the compounds. Their 5% weight loss temperatures ($T_{5\%}$) are collected in Table 4. Compounds DPQ, AcNQ, BrDPQ, and BrAcNQ exhibited high thermal stability with $T_{5\%}$ ranging from 233 to 285 °C. The complete weight loss in the single stage observed by TGA indicates that these values are the temperatures of the onsets of sublimation rather than of the thermal degradation. This observation indicates that films of DPQ, AcNQ, BrDPQ, and BrAcNQ can be obtained by thermal vacuum evaporation.

2.4. Photophysical properties

The absorption spectra of the toluene solutions and the films of DPQ, BrDPQ, AcNQ, and BrAcNQ show the low-energy bands at 320–400 nm (Fig. 6a). These bands mainly result from π-π* transitions in the quinoxaline moiety [48]. The minor redshift of ca. 5–10 nm of the low-energy bands is observed for the toluene solution of BrDPQ when compared to that of DPQ. The electron-withdrawing property of the bromine atoms alters the electronic structure and reduces the optical bandgap of BrDPQ (Fig. 6a). The low-energy bands of AcNQ and BrAcNQ exhibit the vibronic features. These characteristics, apparently, are caused by the rigidity of the molecules. Intermolecular interactions of DPQ, BrDPQ, AcNQ, and BrAcNQ in solid films cause redshifts and low-energy tails in the absorption spectra. The absorption tails are especially obvious for the films of compounds AcNQ and BrAcNQ. These low-energy tails are indications of the compact packing of molecules of AcNQ and BrAcNQ in the solid-state. Apparently, AcNQ and BrAcNQ may form aggregates. This assumption is more relevant to AcNQ, taking into account its emissions peaking at ca. 409 nm (LE emission) and 476 nm (aggregates caused emission [49]) (Fig. 6a and Table 5).

Indeed, relaxation of singlet locally excited (^{1}LE) states of the quinoxaline unit of DPQ, BrDPQ, AcNQ, and BrAcNQ results in emissions with photoluminescence (PL) spectra peaking at 404–427 nm (Fig. 6a and Table 5). Upon deoxygenation, emissions of the films of the compounds at the wavelengths longer than 500 nm were detected due to the

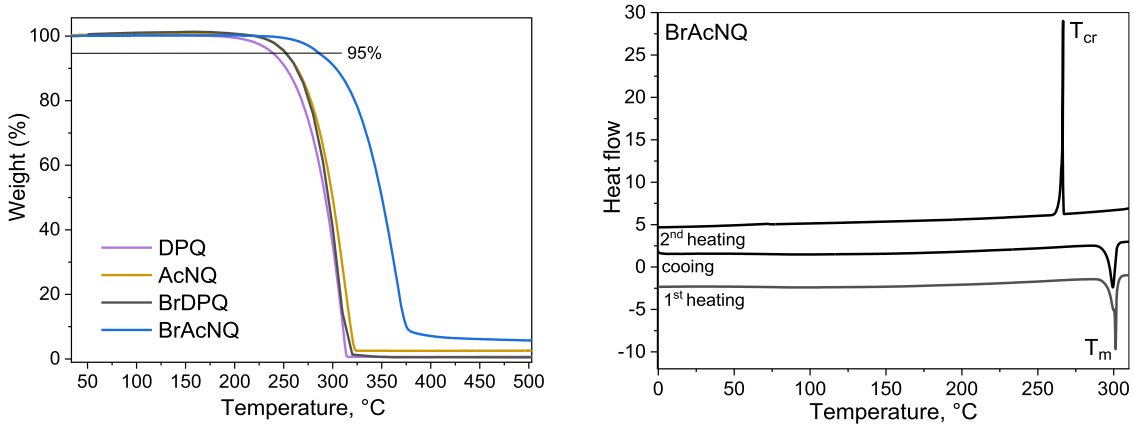

Fig. 5. TGA curves (a) of DPQ, 2BrDPQ, AcNQ and BrAcNQ, DSC curves (b) of BrAcNQ.

relaxation of triplet locally excited (^{3}LE) states. DPQ, BrDPQ, AcNQ, and BrAcNQ show RTP in liquid and solid media when oxygen quenching is minimized. For example, the toluene solutions of BrDPQ and BrAcNQ after deoxygenation exhibit significant increase in emission intensity in the low-energy region. This observation additionally demonstrates the involvement of triplet excitons in the emission. In air, before deoxygenation, the PL spectra of the films resemble to the PL spectra of toluene solutions. The strong suppression of emission by oxygen, along with fluorescence and RTP covering all visible region of the spectrum, positions these materials as excellent candidates for the different applications.

For the investigation of the RTP properties of DPQ, BrDPQ, AcNQ, and BrAcNQ, these compounds were molecularly dispersed in the rigid polymer, Zeonex, at the weight ratio of 1 to 99. The analysis of the molecular dispersions of BrAcNQ in Zeonex with the concentrations of the emitter ranging from 0.1 wt% to 10 wt% confirmed that 1 wt% is the optimal concentration (Fig. S19). Under ambient atmospheric conditions, the PL spectra of the molecular dispersions in Zeonex were similar to the PL spectra of their toluene solutions (Fig. 6b). Fluorescence with the peaks at ca 400 nm was observed. Upon evacuation up to 1×10^{-4} mBar, the compounds showed RTP with PL bands at the wavelengths higher than 500 nm. The films of the solid solutions of DPQ, BrDPQ, AcNQ, and BrAcNQ in Zeonex displayed deep-blue-to-blue fluorescence (FL) and green-to-orange RTP (Fig. 6b). The high single-triplet energy splitting (ΔE_{ST}) values allow to exclude TADF contribution to the emissions of the compounds (Table 5). Corresponding CIE1931 colour coordinates are collected in Table 5. The intense orange RTP of the molecular dispersions of BrDPQ and BrAcNQ in the rigid polymer can be explained by the effect of heavy bromine atoms. They enhance spin-orbit coupling and promote intersystem crossing from ^{1}LE to ^{3}LE, facilitating RTP [50]. The RTP spectrum of AcNQ is characterized by a well-defined vibronic structure, in contrast to the uniform RTP spectrum of DPQ. This difference arises from the rigid and planar molecular structure of AcNQ conferred by the fused acenaphthene rings. The unstructured RTP spectrum of DPQ arises from the flexible molecular structure with rotatable phenyl groups. The time resolved PL measurements revealed very different RTP lifetimes for the molecular dispersions of DPQ, BrDPQ, AcNQ, and BrAcNQ of 19.1, 0.83, 525 and 6.4 ms, respectively (Fig. 6c, Table 5). The different quantum yields of FL (η_{FL}) and RTP (η_{RTP}) were also recorded for the compounds (Table 5, S1). Taking RTP lifetimes (τ_{RTP}) and η_{RTP}, radiative constants (k_{RTP}) for the molecular dispersions of DPQ, BrDPQ, AcNQ, and BrAcNQ in Zeonex were obtained using the following formula.

$$k_{RTP} = \frac{\eta_{RTP}}{\tau_{RTP}} \quad (1)$$

The highest k_{RTP} of 71 s^{-1} was assessed for BrAcNQ. The high η_{RTP} values are typically observed for RTP emitters exhibiting high intersystem crossing (ISC) efficiencies [51]. Assuming that all non-emissive singlets and all emissive triplets are caused by ISC, maximum (k_{ISC}^{max}) and minimum (k_{ISC}^{min}) rate constant of ISC (Table 5) were obtained using the following formulas:

$$k_{ISC}^{min} = \frac{\eta_{RTP}}{\tau_{FL}} \le k_{ISC} \le \frac{1-\eta_{FL}}{\tau_{FL}} = k_{ISC}^{max} \quad (2)$$

All the studied compounds demonstrate relatively high maximum ISC rate constants approaching 1×10^8 s^{-1}. Concerning the minimum ISC rate constants, the highest value of 3×10^7 s^{-1} was obtained for the most efficient RTP emitter BrAcNQ (Table 5Table). Nevertheless, the different photophysical properties of DPQ, BrDPQ, AcNQ, and BrAcNQ offer various insights for the practical applications, some of which are discussed below.

2.5. Emissive tags

The films of DPQ, BrDPQ, AcNQ, and BrAcNQ molecularly dispersed in Zeonex displayed up to the factor of several hundred higher emission intensity after evacuation up to ca. 2×10^{-4} mBar. This observation indicates differences in fluorescence quantum efficiencies η_{FL} and RTP quantum yields η_{RTP} (Table 5, S1). For example, the film of the molecular dispersion of BrAcNQ showed very low η_{FL} of 0.05 % and high η_{RTP} of 45.52 % (Table S1) [12]. The low η_{FL} and high η_{RTP} values are the main requirements for materials intended for luminescence tags [52]. RTP materials with high P2F parameters (Eq. 3) ensure high contrast between emissive and non-emissive areas of the emissive tags [30].

$$\mathrm{P2F} = \frac{\eta_{RTP}}{\eta_{FL}} \quad (3)$$

The authors of ref [52] screened more than 290 RTP emitters, and did not find compounds with P2F parameters higher than 39. They developed efficient luminescent tags using 4,4′-dithianthrene-1-yl-benzophenone (BP-2TA) as RTP emitter characterized by maximum P2F of 18. In addition, BP-2TA showed the intensity-averaged RTP lifetime of 30 ms. Short RTP lifetime is required for tag materials allowing fast on/off switching of written information.

In our case, the maximum P2F of 910 was obtained for BrAcNQ (1 wt. %) molecularly dispersed in Zeonex. The molecular mixture showed bright and fast turn-on/off response (Fig. 7a) due to its high η_{RTP} of 45.52%, short RTP lifetime of 6.4 ms and the relatively high k_{RTP} of 71 s^{-1}. Meanwhile, the polymer molecularly doped with BP-2TA showed η_{RTP} of 21%, the RTP lifetime of 30 ms and k_{RTP} of 7 s^{-1} (Fig. 6c and Table 5). Due to the perfect combination of high P2F, low η_{FL}, high η_{RTP} and moderate τ_{RTP} of Zeonex molecularly doped with BrAcNQ, this compound was used for the fabrication of luminescent tags. To save information “ktu” to the tags, the films of the molecular mixture of BrAcNQ (1 wt%) and Zeonex were excited by strong UV radiation (395 nm)

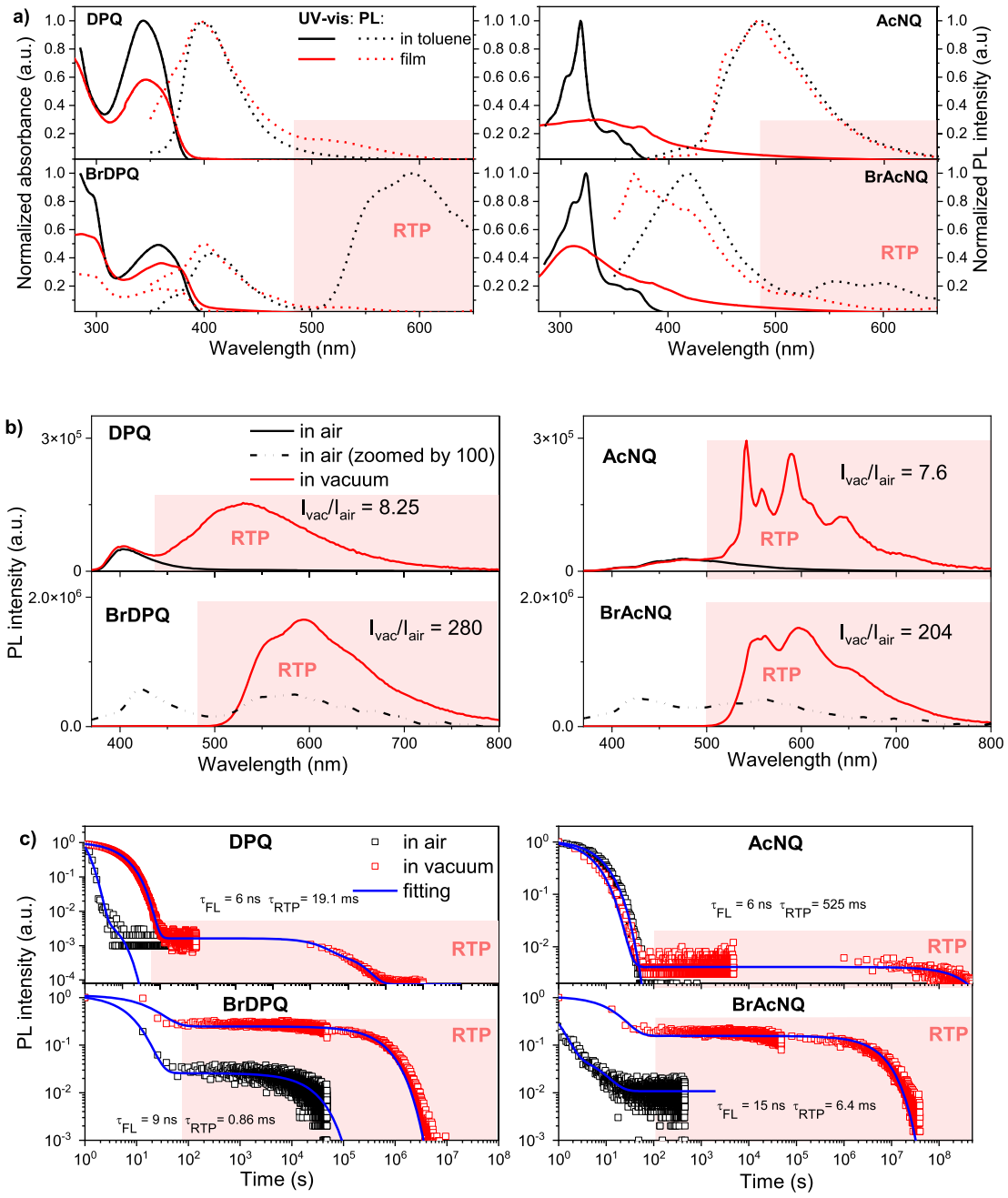

Fig. 6. Absorption and PL spectra of dilute toluene solutions (10-5 M) and films of DPQ, BrDPQ, AcNQ, and BrAcNQ (a). PL spectra (b) and PL decay curves (c) of molecular dispersions (1 wt%) of DPQ, BrDPQ, AcNQ, and BrAcNQ in Zeonex, recorded in air and vacuum.

according to the procedure described elsewhere (Fig. 7b)[30]. The information was well reproduced using weak UV excitation (355 nm) (Fig. 7b). It should be noted that compounds BrDPQ and BrAcNQ with high η_{RTP} and P2F can also be used for imaging. For example, the drop-casted films of BrDPQ and BrAcNQ molecularly dispersed in Zeonex showed considerably better resolution (contrast between bright orange (RTP) and dark (fluorescence) areas) than the previously developed RTP materials [53].

2.6. Single-emitter white OLEDs

The whitish emission was observed for AcNQ (1 wt.%) molecularly dispersed in Zeonex at "O_2 off" due to the overlapping of blue FL and yellow RTP (Fig. 8a). The whitish emission was observed for OLEDs with the emitting layers of compounds DPQ, BrDPQ, AcNQ, and BrAcNQ molecularly dispersed in host tris(4-carbazoyl-9-yl-phenyl)amine (TCTA) (Table 6). This property may be useful for the development of single-component OLEDs for lighting applications [6]. For the verification of this assumption, the synthesized quinoxaline derivatives were tested as emitters in solution-processable OLEDs. The structure of the developed devices was as follows: poly(3,4-ethylenedioxythiophene): polystyrene sulfonate (PEDOT:PSS) (40 nm)/EML(30 nm)/diphenyl [4-(triphenylsilyl)phenyl]phosphine oxide (TSPO1) (4 nm)/ 2,2′,2″-(1,3,5-benzinetriyl)-tris(1-phenyl-1-*H*-benzimidazole) (TPBi) (40 nm)/ lithium fluoride (LiF)/Al. Light-emitting layers (EMLs) consisted of 1 % wt. of quinoxaline derivatives molecularly dispersed in the host (TCTA). The layers of PEDOT:PSS and EML were spin-coated. The host TCTA was chosen taking into account its large band gap ($E_g = 3.3$ eV) and emission

Table 5
Photophysical parameters of DPQ, BrDPQ, AcNQ, and BrAcNQ.

Compound	Media	DPQ	BrDPQ	AcNQ	BrAcNQ
λ_{ABS}, nm	Toluene	344	358	318, 349, 366	324, 352, 369
λ_{FL}, nm	Zeonex	404	422	409, 476	427
λ_{RTP}, nm		535	596	543, 560, 589, 644	555, 598, 650
ΔE_{ST}, eV		0.75	0.86	0.75	0.67
τ_{FL}, ns		14	6	9	15
τ_{RTP}, ms		19.1	0.83	525	6.4
η_{FL}, %		0.28	0.32	0.29	0.05
η_{RTP}, %		2.18	32.18	4.79	45.52
k_{RTP}, s^{-1}		1.1	0.39	0.09	71
k_{ISC}^{max}, s^{-1}		0.71×10^8	1.65×10^8	1.11×10^8	0.67×10^8
k_{ISC}^{min}, s^{-1}		0.16×10^7	5.4×10^7	0.53×10^7	3×10^7
P2F		7.8	101	17	910
$CIE1931_{FL}$, (x, y)		(0.484, 0.452)	(0.151, 0.035)	(0.197, 0.263)	(0.140, 0.070)
$CIE1931_{RTP}$, (x, y)		(0.310, 0.432)	(0.513, 0.478)	(0.447, 0.469)	(0.509, 0.484)

in the UV region, which well overlaps with the absorption of the studied emitters (Fig. 6a). TCTA is characterized by high T_g of 151°C [47]), appropriate HOMO/LUMO energy levels and good charge-transporting properties [54,55]. The developed OLEDs A1, A2, A3 and A4 contained emitters DPQ, BrDPQ, AcNQ, and BrAcNQ, respectively.

For the understanding of the nature of electroluminescence of DPQ, BrDPQ, AcNQ, and BrAcNQ-based OLEDs, EL spectra of devices A1–4, along with the PL spectra of EMLs, were recorded (Fig. 10). The EL spectra of OLEDs A1–4 consisted of several bands which correlated well with the PL spectra of the emitters dispersed in the different media (Fig. 6b, 8a, c). The emission bands observed at 400–480 nm originated from the fluorescence of the emitters (Fig. S20). They are similar to fluorescence bands of their dilute solutions, or of solid films of the molecular dispersions (1 wt%) of DPQ, BrDPQ, AcNQ, and BrAcNQ in Zeonex or TCTA. The emissions at the wavelengths longer than 480 nm are attributed to the RTP of molecular dispersions of quinoxaline-based derivatives. This statement is in good agreement with the long-lived electroluminescence detected at 500 and 600 nm from transient electroluminescent (TREL) plots of devices A1-4 recorded in a microsecond range. The EL decay curves of devices A2 and A4 containing brominated quinoxaline derivatives BrDPQ and BrAcNQ as emitters showed two long-lived emission components. The obtained TREL plot is consistent with the RTP characteristics of the molecular dispersions of emitters BrDPQ and BrAcNQ in Zeonex.

The lifetimes of electroluminescence were found to be of 0.82 ms for device A2 and of 4.23 ms for device A4. The lifetimes of electroluminescence were not estimated for devices A1 and A3, containing emitters DPQ and AcNQ, since they exhibited ultralong phosphorescence without the slope in the millisecond range (Fig. 8b). These TREL results are consistent with the results of PL decay measurements of the compounds molecularly dispersed in a TCTA host (Fig. 8d). The bromine-containing compounds BrDPQ and BrAcNQ exhibited relatively short phosphorescence lifetimes. In the same time range, the samples with non-brominated compounds DPQ and AcNQ did not show any phosphorescence. Thus, molecular dispersions of DPQ and AcNQ in TCTA are characterized by ultralong phosphorescence lifetimes similar to those of Zeonex polymer molecularly doped with DPQ or AcNQ (Fig. 8d).

The overlapping of blue fluorescence and red phosphorescence in electroluminescence of devices A1 and A2 lead to near to white emission, with Commission Internationale *de l'éclairage* (CIE 1931) coordinates close to white coordinates (0.33; 0.33) (Fig. 9b and Table 6). The colour rendering indices (CRI) of A2 and A4 exceeded 80. OLEDs A1-4 showed relatively low turn-on voltages ranging from 3.3 to 3.8 V. This observation can be explained by the well-chosen functional layers of the devices preventing energy barriers for holes and electrons (Fig. 9a and c). The single-emitter white RTP based OLEDs with the synthesized quinoxaline derivatives showed relatively low maximum EQEs ranging from 0.44 to 0.93% (Fig. 9d and Table 6). These values are slightly higher than those of the recently published single molecular white OLEDs [7]. Nevertheless, they are beloved of the state-of-the-art EQE values of OLEDs reaching over 40% without outcoupling [4]. Such results are mainly attributed to the quenching of RTP of the emitters molecularly dispersed in TCTA, causing lower PLQYs (up to 4.62 %) in comparison to those observed for the films of the molecular dispersions in Zeonex (Table S1). This observation suggests the design of OLED hosts, which can enhance the efficiency of RTP emitters. In addition, the fluorescence of DPQ, BrDPQ, AcNQ, and BrAcNQ is very weak in comparison to the RTP component (Fig. 8a). This observation suggests the design of RTP emitters with the comparable efficiency of fluorescence and RTP.

Taking into account the colour quality of white electroluminescence characterized by CRI of 80 and 83 observed for BrDPQ and BrAcNQ-based devices, respectively (Table 6), it can be concluded that the compounds are suitable for single-emitter white OLEDs. However, their EQE values are rather low in comparison to those of state-of-the-art multicomponent OLEDs. However, there are more promising applications of the molecular dispersions of DPQ, BrDPQ, AcNQ, and BrAcNQ in polymeric host Zeonex, e.g. for emissive tags or oxygen sensors.

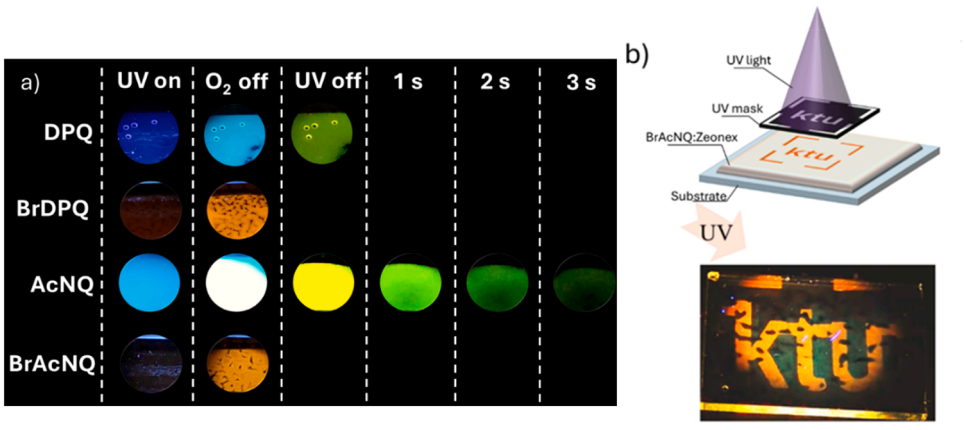

Fig. 7. Molecular dispersions (1 wt%) of DPQ, BrDPQ, AcNQ, and BrAcNQ in Zeonex under different UV excitation conditions (a). "UV on" - weak UV excitation, "O2 off" - strong UV excitation, and "UV off", "1 s", "2 s", "3 s" - the emissions at different times after UV switching off. Schematic visualization of the local activation of RTP of the molecular dispersion of BrAcNQ in Zeonex by intense UV radiation through the shadow mask [30] and reproduction of the written information using weak UV radiation (b).

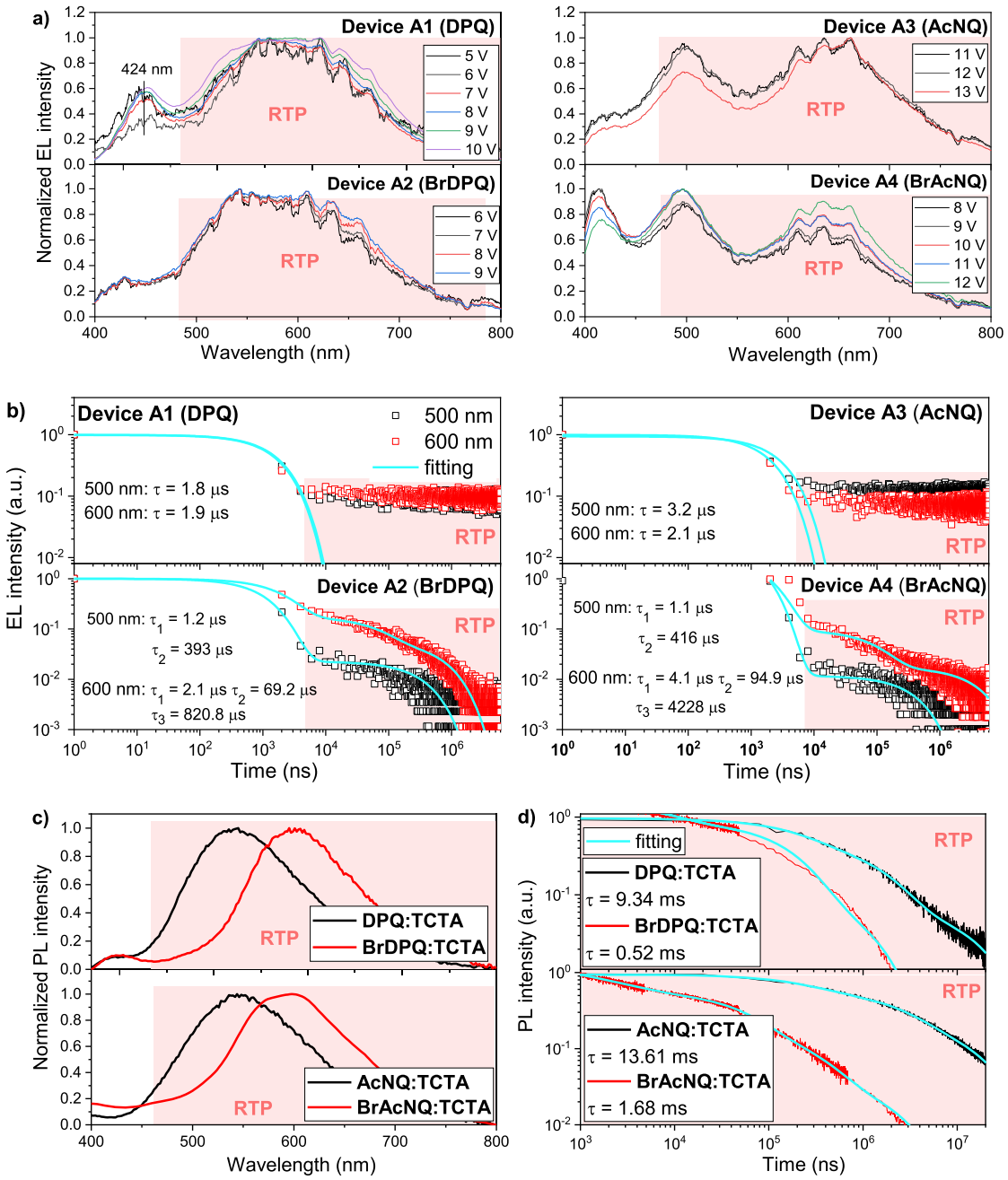

Fig. 8. EL spectra (a) recorded at the different voltages and TREL plots (b) taken at 500 and 600 nm for devices A1–4. PL spectra (c) and PL decay curves (d) of molecular dispersions (1 wt%) of DPQ, BrDPQ, AcNQ, and BrAcNQ in TCTA, recorded in vacuum.

Table 6
Characteristics of OLEDs with the structure of PEDOT:PSS/EML/TSPO1(4nm)/TPBi(40nm)/LiF/Al.

Device	EML	V_{ON}, V	Brightness, cd/m^2	CE, cd/A	PE, lm/W	EQE, %	CCT, K	CIE1931,(x; y)	CRI
A1	DPQ(1% wt.) TCTA	3.8	46	0.62	0.40	0.44	6249	0.32; 0.31	71
A2	BrDPQ(1% wt.) TCTA	3.5	112	1.82	1.59	0.93	3825	0.41; 0.45	83
A3	AcNQ(1% wt.) TCTA	3.3	178	1.11	1.00	0.88	4247	0.37; 0.37	77
A4	BrAcNQ(1% wt.) TCTA	3.5	64	1.10	0.84	0.55	4210	0.38; 0.42	80

2.7. Oxygen sensing

For verification of the studied compounds as oxygen sensing materials, their RTP properties were studied under the mixtures of oxygen and nitrogen of the different compositions. The PL spectra of the selected compounds (1 % wt.) molecularly doped in Zeonex were recorded (Figs. 10a and S14). The Stern-Volmer constants (K_{SV}) were calculated from the collected data. The Stern Volmer plots were non-linear for all the samples, as shown in Fig. 10b, indicating the presence of at least two main luminophore species. To determine the K_{SV} values, Eq. 4 was used [56]:

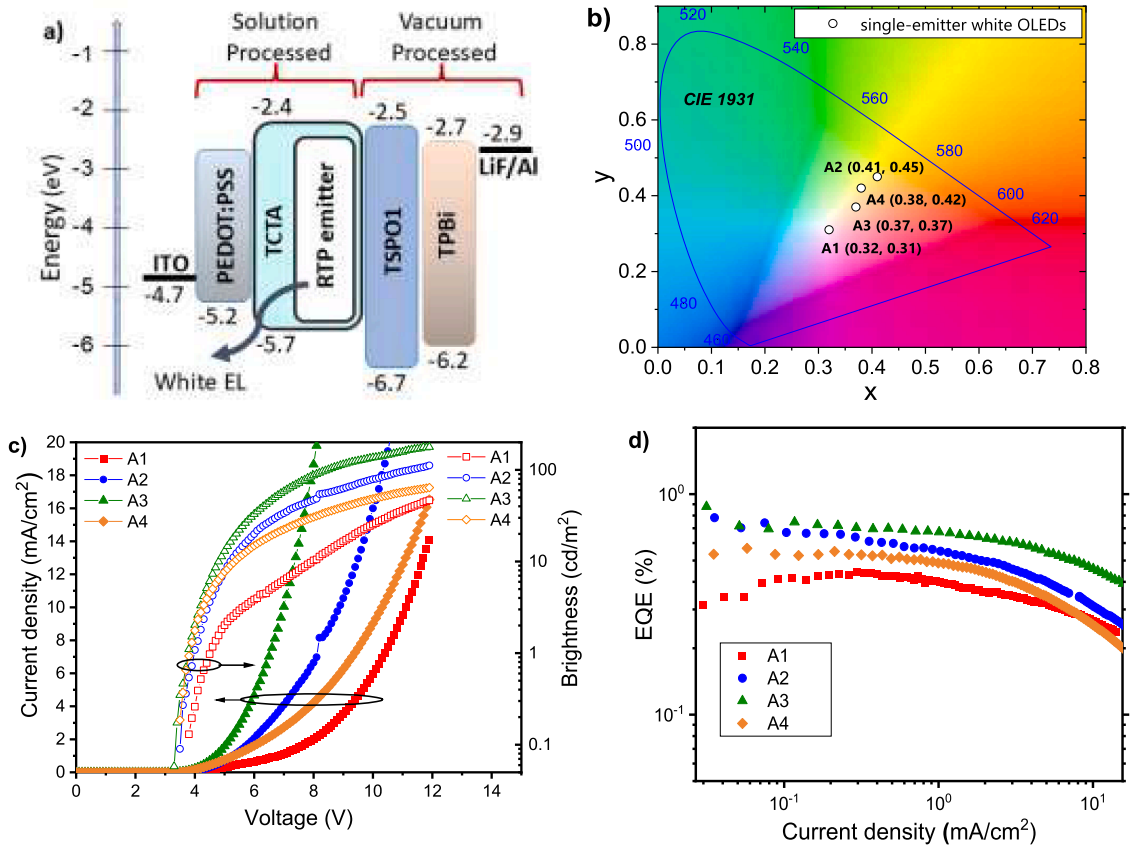

Fig. 9. Equilibrium energy diagrams (a), CIE1931 color coordinate diagrams (b), current density and brightness characteristics versus of voltage plots (c), EQE versus current density plots (d) of devices A1–4.

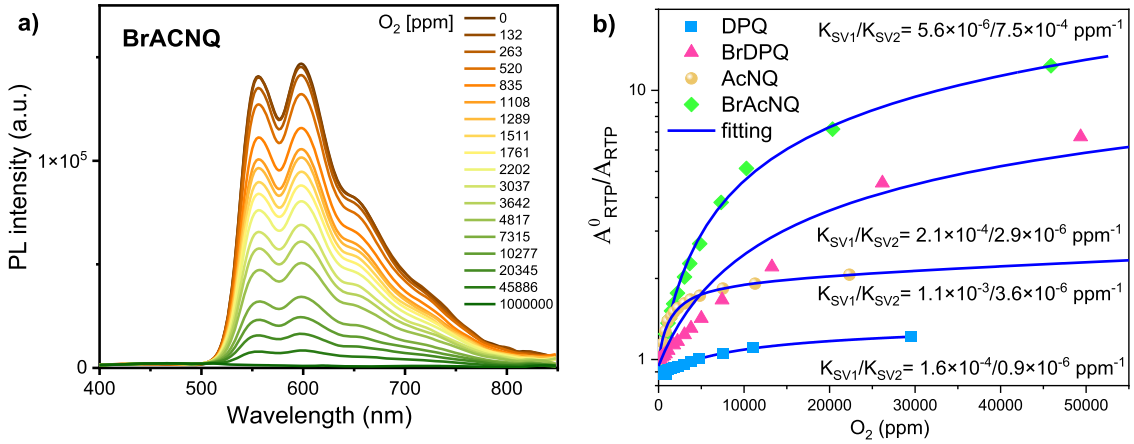

Fig. 10. PL spectra (a) of molecularly dispersion (1 wt%) of BrACNQ in Zeonex and Stern Volmer plots (b) of molecular dispersions (1 wt%) of DPQ, BrDPQ, AcNQ, and BrAcNQ in Zeonex.

$$\frac{A_0^{RTP}}{A} = \left[\sum_{i=1}^{n} \frac{f_i}{(1 + K_{SVi}[O_2])}\right]^{-1} \quad (4)$$

where A_0^{RTP} is the integrated area of PL spectrum recorded under vacuum, A is the integrated area of PL spectrum recorded at the different concentrations of oxygen, f_i is fractional intensity.

Stern Volmer plots were well fitted using *n* of 2 (Fig. 10b). As a result, two values of fractional intensities (f_1 and f_2) and Stern-Volmer constants (K_{SV1} and K_{SV2}) were obtained. The best oxygen sensitivity with K_{SV} values of 5.6×10^{-4} ppm^{-1} and 7.46×10^{-6} ppm^{-1} was estimated for BrAcNQ molecularly doped in Zeonex characterized by the highest η_{RTP} of 45.52 %. The f for both the species were found to be of 0.954 and 0.046. The higher K_{SV1} value of 5.6×10^{-4} ppm is attributed to RTP. The presence of the second K_{SV} value can be explained by oxygen penetration into the layer of Zeonex molecularly doped with BrAcNQ. The layer of compound BrDPQ molecularly dispersed in Zeonex showed the similar results. The values of K_{SV1} and K_{SV2} were found to be of 2.07×10^{-4} ppm^{-1} and 2.94×10^{-6} ppm^{-1}, and f values were of 0.907 and 0.093, respectively. The comparison of the performance of these two samples, allows to conclude that the probe containing compound BrACNQ has slightly better oxygen-sensing properties than the sample with BrDPQ.

This observation is in good agreement with the slightly more efficient RTP of the polymer films containing BrACNQ than of the samples with BrDPQ. The films of Zeonex molecularly doped with BrACNQ showed higher η_{RTP}, τ_{RTP} and k_{RTP} values than the corresponding films containing BrDPQ (Table 5).

The calculated K_{SV} values for the film of Zeonex molecularly doped with DPQ were found to be of 1.6×10^{-4} ppm^{-1} and 9.3×10^{-7} ppm^{-1}, and the f values were of 0.336 and 0.664, respectively. The calculated K_{SV} values for the film of Zeonex molecularly doped with AcNQ were of 1.1×10^{-3} ppm^{-1} and 3.6×10^{-6} ppm^{-1}, and the f values were of 0.511 and 0.489, respectively. As the f values were close for the samples of both the compounds, the overall sensitivity to oxygen is almost equally impacted by both emitting species. It should be noted that the highest K_{SV1} value of 1.1×10^{-3} ppm^{-1}, which is attributed to RTP, was obtained for the film of Zeonex molecularly doped with AcNQ (Fig. 10b). These films showed the highest K_{SV} values not only in comparison to the whole series but they are also among the highest values for the published organic RTP oxygen sensing materials [57,58]. This finding can be attributed the longest RTP lifetime of 525 ms observed for the films containing AcNQ (Fig. 6c, Table 5). The value of η_{RTP} of AcNQ molecularly dispersed in Zeonex is much lower than those of the corresponding samples of BrACNQ and BrDPQ. Nevertheless, this observation creates prerequisite for the development of novel RTP emitters with high η_{RTP} η_{RTP} and τ_{RTP} values for oxygen sensing applications.

3. Conclusions

For the applications of organic triplet emitters, it is essential that they simultaneously exhibit high quantum yields and optimal lifetimes of room temperature phosphorescence as well as high contrast between the informative and background signals. Quinoxaline derivatives with both rigid and flexible molecular structures, with heavy bromine atoms or without them, exhibit from green to orange room temperature phosphorescence with quantum yields of up to 45.6% and lifetimes spanning from 0.83 to 525 ms. One of the studied compounds molecularly doped in the rigid polymer exhibit quantum yield of room temperature phosphorescence higher by the factor of 910 times relative to fluorescence quantum yield. This property allows to achieve the state-of-art performance in luminescent tags and morphological imaging. The fast turn-on/off response of luminescence tags is achieved due to the relatively high radiative constants of the compounds. The solutions processed OLEDs with the emitting layers of the synthesized compounds showed whitish electroluminescence with the colour coordinates of (0.32, 0.31) close to those of natural white emission (0.33, 0.33). The long-lived room temperature phosphorescence of the quinoxaline derivative with rigid molecular structure and without bromine atoms allows to obtain one of the highest Stern-Volmer constants of 1.1×10^{-3} ppm^{-1} for organic sensing materials of oxygen. The quinoxaline derivatives with the different molecular structures exhibit diverse potential for various applications, primarily due to their differing emission colours, quantum yields, and lifetimes of fluorescence and room temperature phosphorescence.

CRediT authorship contribution statement

Mohamed Abdella: Writing – original draft, Visualization, Investigation, Formal analysis, Data curation. **Matas Guzauskas:** Visualization, Validation, Methodology, Investigation. **Jurate Simokaitiene:** Visualization, Supervision, Methodology, Investigation, Conceptualization. **Asta Dabuliene:** Investigation, Data curation. **Monika Cekaviciute:** Supervision, Methodology, Formal analysis. **Dmytro Volyniuk:** Writing – original draft, Visualization, Validation, Supervision, Project administration, Investigation, Funding acquisition, Conceptualization. **Vitaly E. Matulis:** Writing – original draft, Supervision, Investigation. **Ekaterina G. Ragoyja:** Validation, Supervision. **Juozas V. Grazulevicius:** Writing – review & editing, Validation, Supervision, Project administration, Funding acquisition.

Declaration of competing interest

The authors declare the following financial interests/personal relationships which may be considered as potential competing interests Juozas Vidas Grazulevicius reports financial support was provided by Research Council of Lithuania. Jouzas Vidas Grazulevicius reports a relationship with Kaunas University of Technology that includes: employment. If there are other authors, they declare that they have no known competing financial interests or personal relationships that could have appeared to influence the work reported in this paper.

Acknowledgements

This work has received funding from the Research Council of Lithuania (LMTLT), agreement No S-A-UEI-23-1 (22-12-2023). This work also received support from Horizon Europe, the European Union's framework programme for research and innovation (R&I) for 2021-2027, project HELIOS, grant agreement No 101155017.

Supplementary materials

Supplementary material associated with this article can be found, in the online version, at doi:10.1016/j.rineng.2026.109560.

Data availability

Data are avalible in the supporting information.

References

[1] T. Tsutsui, M.-J. Yang, M. Yahiro, K. Nakamura, T. Watanabe, T. Tsuji, Y. Fukuda, T. Wakimoto, S. Miyaguchi, High quantum efficiency in organic light-emitting devices with iridium-complex as a triplet emissive center, Jpn. J. Appl. Phys. 38 (1999) L1502, https://doi.org/10.1143/JJAP.38.L1502.

[2] OLED-Info | OLED industry portal, (n.d.). https://www.oled-info.com/(accessed, October 22, 2025.

[3] P. Li, W. Li, Y. Zhang, P. Zhang, X. Wang, C. Yin, R. Chen, Recent progress of thermally activated delayed fluorescent materials with narrowband red, green, and blue (RGB) emission, ACS. Mater. Lett. 6 (2024) 1746–1768, https://doi.org/10.1021/acsmaterialslett.4c00178.

[4] H.S. Kim, H.J. Cheon, S.H. Lee, J. Kim, S. Yoo, Y.-H. Kim, C. Adachi, Advancing efficiency in deep-blue OLEDs: exploring a machine learning-driven multiresonance TADF molecular design, Sci. Adv. 11 (2025) eadr1326, https://doi.org/10.1126/sciadv.adr1326.

[5] Z. Xie, C. Chen, S. Xu, J. Li, Y. Zhang, S. Liu, J. Xu, Z. Chi, White-light emission strategy of a single organic compound with aggregation-induced emission and delayed fluorescence properties, Angew. Chem. Int. Ed. Engl. 54 (2015) 7181–7184, https://doi.org/10.1002/anie.201502180.

[6] M. Zhang, W. Li, S.W. Zhang, M. Ng, C. Wu, M.C. Tang, Y. Wu, C. Yang, H. Meng, J. Zhao, C. He, G. Wei, F. Kang, Efficient single-molecular white-light emission for iridium-based photoluminescent and electroluminescent white OLEDs, Cell Rep. Phys. Sci. 4 (2023) 101684, https://doi.org/10.1016/J.XCRP.2023.101684.

[7] M. Liu, H. Hao, G. Liao, C. Li, K. Liu, N. Wang, Q. Niu, X. Yin, M. Liu, G. Liao, C. Li, K. Liu, N. Wang, X. Yin, H. Hao, Q. Niu, Boron-containing molecules with fluorescence-phosphorescence dual-emission for mechanochromism and single molecular white light-emitting diodes, Adv. Opt. Mater. 11 (2023) 2202918, https://doi.org/10.1002/ADOM.202202918.

[8] C. Zhou, S. Zhang, Y. Gao, H. Liu, T. Shan, X. Liang, B. Yang, Y. Ma, C. Zhou, S. Zhang, Y. Gao, H. Liu, T. Shan, B. Yang, X. Liang, Y. Ma, Ternary emission of fluorescence and dual phosphorescence at room temperature: A single-molecule white light emitter based on pure organic aza-aromatic material, Adv. Funct. Mater. 28 (2018) 1802407, https://doi.org/10.1002/ADFM.201802407.

[9] Z. Wu, H. Choi, Z.M. Hudson, Achieving white-light emission using organic persistent room temperature phosphorescence, Angew. Chem. Int. Ed. Engl. 62 (2023) e202301186, https://doi.org/10.1002/anie.202301186.

[10] Z. Yang, Z. Fu, H. Liu, M. Wu, N. Li, K. Wang, S.T. Zhang, B. Zou, B. Yang, Pressure-induced room-temperature phosphorescence enhancement based on purely organic molecules with a folded geometry, Chem. Sci. 14 (2023) 2640–2645, https://doi.org/10.1039/D3SC00172E.

[11] L. Volyniuk, D. Gudeika, A.A. Panchenko, B.F. Minaev, M. Mahmoudi, J. Simokaitiene, A. Bucinskas, D. Volyniuk, J.V. Grazulevicius, Single-molecular white emission of organic thianthrene-based luminophores exhibiting efficient fluorescence and room temperature phosphorescence induced by halogen atoms,

ACS. Sustain. Chem. Eng. 11 (2023) 16914–16925, https://doi.org/10.1021/acssuschemeng.3c04011.
[12] M. Stanitska, D. Volyniuk, B. Minaev, H. Agren, J.V. Grazulevicius, Molecular design, synthesis, properties, and applications of organic triplet emitters exhibiting blue, green, red and white room-temperature phosphorescence, J. Mater. Chem. C. Mater. 12 (2024) 2662–2698, https://doi.org/10.1039/D3TC04514E.
[13] Z. Chen, Q. Gu, M. Li, W. Qiu, Y. Jiao, X. Peng, W. Xie, D. Liu, K. Liu, Z. Yang, S. J. Su, Extended Π-conjugation toward efficient orange purely organic phosphorescence OLEDs, Adv. Opt. Mater. 12 (2024) 2302503, https://doi.org/10.1002/ADOM.202302503.
[14] Y. Zhang, Z. Wang, Y. Su, Y. Zheng, W. Tang, C. Yang, H. Tang, L. Qu, Y. Li, Y. Zhao, Simple vanilla derivatives for long-lived room-temperature polymer phosphorescence as invisible security inks, Research. (Wash. D. C) (2021) 8096263, https://doi.org/10.34133/2021/8096263, 2021.
[15] L. Skhirtladze, K. Leitonas, A. Bucinskas, K.L. Woon, D. Volyniuk, R. Keruckienė, M. Mahmoudi, M. Lapkowski, A. Ariffin, J.V. Grazulevicius, Turn on of room temperature phosphorescence of donor-acceptor-donor type compounds via transformation of excited states by rigid hosts for oxygen sensing, Sens. Actuators. B Chem. 380 (2023) 133295, https://doi.org/10.1016/j.snb.2023.133295.
[16] J. Gao, Y. Zhao, X. You, Y. Geng, G. Shan, Z. Su, Y. Gao, Theoretical search of a simple characteristic for long-lived organic room-temperature phosphorescence materials with H aggregation, J. Mater. Chem. C. Mater. 10 (2022) 5425–5432, https://doi.org/10.1039/D2TC00518B.
[17] M. Ji, X. Ma, Recent progress with the application of organic room-temperature phosphorescent materials, Ind. Chem. Mater. 1 (2023) 582–594, https://doi.org/10.1039/D3IM00004D.
[18] Q. Chen, L. Qu, H. Hou, J. Huang, C. Li, Y. Zhu, Y. Wang, X. Chen, Q. Zhou, Y. Yang, C. Yang, Long lifetimes white afterglow in slightly crosslinked polymer systems, Nat. Commun. 15 (2024) 1–11, https://doi.org/10.1038/S41467-024-47378-2;TECHMETA.
[19] L. Gao, J. Huang, L. Qu, X. Chen, Y. Zhu, C. Li, Q. Tian, Y. Zhao, C. Yang, Stepwise taming of triplet excitons via multiple confinements in intrinsic polymers for long-lived room-temperature phosphorescence, Nat. Commun. 14 (2023) 1–9, https://doi.org/10.1038/S41467-023-43133-1;TECHMETA.
[20] C. Wang, Y. Zhang, Z. Wang, Y. Zheng, X. Zheng, L. Gao, Q. Zhou, J. Hao, B. Pi, Q. Li, C. Yang, Y. Li, K. Wang, Y. Zhao, Photo-induced dynamic room temperature phosphorescence based on triphenyl phosphonium containing polymers, Adv. Funct. Mater. 32 (2022) 2111941, https://doi.org/10.1002/adfm.202111941.
[21] L. Gao, Y. Zhang, X. Chen, Y. Zheng, X. Zheng, C. Wang, Z. Wang, J. Hao, Q. Tian, X. Yu, C. Yang, Y. Li, Y. Zhao, Water-induced blue-green variable nonconventional ultralong room temperature phosphorescence from cross-linked copolymers via click chemistry, Adv. Opt. Mater. 9 (2021) 2101284, https://doi.org/10.1002/adom.202101284.
[22] M. Tsuboi, S. Nakamura, S. Nandi, P. de Silva, Y. Takeda, M. Miura, Syntheses and room temperature phosphorescence properties of dibenzobenzodithiophenes and dibenzothiophenes, Bull. Chem. Soc. Jpn. 94 (2021) 2498–2504, https://doi.org/10.1246/bcsj.20210225.
[23] Z. Xu, D. Hean, C. Climent, D. Casanova, M.O. Wolf, Switching between TADF and RTP: anion-regulated photoluminescence in organic salts and co-crystals, Mater. Adv. 2 (2021) 5777–5784, https://doi.org/10.1039/D1MA00314C.
[24] C.Chen Kenry, B. Liu, Enhancing the performance of pure organic room-temperature phosphorescent luminophores, Nat. Commun. 10 (2019) 2111, https://doi.org/10.1038/s41467-019-10033-2.
[25] H. Hou, H. Wang, M. He, Q. Li, X. Wang, F. Guo, Q. Chen, L. Qu, C. Yang, Thermal annealing effects on long-lived fluorenol room temperature phosphorescence for styrene detection, Angew. Chem. Int. Ed. Engl. 63 (2024) e202411323, https://doi.org/10.1002/anie.202411323.
[26] H. Wang, H. Ma, N. Gan, K. Qin, Z. Song, A. Lv, K. Wang, W. Ye, X. Yao, C. Zhou, X. Wang, Z. Zhou, S. Yang, L. Yang, C. Bo, H. Shi, F. Huo, G. Li, W. Huang, Z. An, Abnormal thermally-stimulated dynamic organic phosphorescence, Nat. Commun. 15 (2024) 2134, https://doi.org/10.1038/s41467-024-45811-0.
[27] K. Chen, Y. Luo, M. Sun, C. Liu, M. Jia, C. Fu, X. Shen, C. Li, X. Zheng, X. Pu, Y. Huang, Z. Lu, Acquiring charge-transfer-featured single-molecule ultralong organic room temperature phosphorescence via through-space electronic coupling, Angew. Chem. Int. Ed. Engl. 63 (2024) e202314447, https://doi.org/10.1002/anie.202314447.
[28] W. Ye, H. Ma, H. Shi, H. Wang, A. Lv, L. Bian, M. Zhang, C. Ma, K. Ling, M. Gu, Y. Mao, X. Yao, C. Gao, K. Shen, W. Jia, J. Zhi, S. Cai, Z. Song, J. Li, Y. Zhang, S. Lu, K. Liu, C. Dong, Q. Wang, Y. Zhou, W. Yao, Y. Zhang, H. Zhang, Z. Zhang, X. Hang, Z. An, X. Liu, W. Huang, Confining isolated chromophores for highly efficient blue phosphorescence, Nat. Mater. 20 (2021) 1539–1544, https://doi.org/10.1038/S41563-021-01073-5;TECHMETA.
[29] N. Gan, X. Zou, M. Dong, Y. Wang, X. Wang, A. Lv, Z. Song, Y. Zhang, W. Gong, Z. Zhao, Z. Wang, Z. Zhou, H. Ma, X. Liu, Q. Chen, H. Shi, H. Yang, L. Gu, Z. An, W. Huang, Organic phosphorescent scintillation from copolymers by X-ray irradiation, Nat. Commun. 13 (2022) 3995, https://doi.org/10.1038/s41467-022-31554-3.
[30] H. Thomas, T. Achenbach, I.M. Hodgkinson, Y. Spoerer, I. Kuehnert, C. Dornack, K. S. Schellhammer, S. Reineke, Room temperature phosphorescence from natural, organic emitters and their application in industrially compostable programmable luminescent tags, Adv. Mater. 36 (2024) e2310674, https://doi.org/10.1002/adma.202310674.
[31] E. Skuodis, K. Leitonas, A. Panchenko, L. Volyniuk, J. Simokaitienė, R. Keruckienė, D. Volyniuk, B.F. Minaev, J.V. Gražulevičius, Very sensitive probes for quantitative and organoleptic detection of oxygen based on conformer-induced room-temperature phosphorescence enhancement of the derivative of triazatruxene and phenothiazine, Sens. Actuators. B Chem. 373 (2022) 132727, https://doi.org/10.1016/j.snb.2022.132727.
[32] Q. Wang, X.-L. Xu, M.-Y. Zhu, Y.-P. Du, Y.-J. Ma, J.-H. Li, G.-M. Wang, Integrating three-primary-color and white long-lasting afterglows in triphenylene-doped polymers for time/space-resolved applications, Chem. Eng. J. 507 (2025) 160535, https://doi.org/10.1016/j.cej.2025.160535.
[33] H. Ma, Y. Qin, N. Zhang, H. Mu, J. Liu, S. Xue, Q. Sun, W. Yang, Realizing multicolor, 3D-printable ultralong room temperature phosphorescence PLA materials via regulating the π-system of aryl-annulated carbazoles, Adv. Mater. 37 (2025) 2510443, https://doi.org/10.1002/adma.202510443.
[34] A.H. Bansode, G. Suryavanshi, Iodine-mediated oxidative rearrangement of α,β-unsaturated diaryl ketones: A facile access to 1,2-diaryl diketones, ACS. Omega 4 (2019) 9636–9644, https://doi.org/10.1021/ACSOMEGA.9B00833/ASSET/IMAGES/LARGE/AO-2019-00833Y_0007.JPEG.
[35] H. Hussain, S. Specht, S.R. Sarite, M. Saeftel, A. Hoerauf, B. Schulz, K. Krohn, A new class of phenazines with activity against a chloroquine resistant plasmodium falciparum strain and antimicrobial activity, J. Med. Chem. 54 (2011) 4913–4917, https://doi.org/10.1021/JM200302D/SUPPL_FILE/JM200302D_SI_001.PDF.
[36] H.S. Yu, X. He, S.L. Li, D.G. Truhlar, MN15: A Kohn–Sham global-hybrid exchange–correlation density functional with broad accuracy for multi-reference and single-reference systems and noncovalent interactions, Chem. Sci. 7 (2016) 5032–5051, https://doi.org/10.1039/C6SC00705H.
[37] B. Zhang, H. Xu, Y. Xia, J. Wen, M. Zhu, Effect of void-carbon on blue-shifted luminescence in TADF molecules by theoretical simulations, Front. Chem. 11 (2023) 1–10, https://doi.org/10.3389/fchem.2023.1094574.
[38] A.V. Marenich, C.J. Cramer, D.G. Truhlar, Universal solvation model based on solute electron density and on a continuum model of the solvent defined by the bulk dielectric constant and atomic surface tensions, J. Phys. Chem. B 113 (2009) 6378–6396, https://doi.org/10.1021/jp810292n.
[39] R. Cammi, B. Mennucci, Linear response theory for the polarizable continuum model, J. Chem. Phys. 110 (1999) 9877–9886, https://doi.org/10.1063/1.478861.
[40] D.J.F.M.J. Frisch, G.W. Trucks, H.B. Schlegel, G.E. Scuseria, M.A. Robb, J. R. Cheeseman, G. Scalmani, V. Barone, G.A. Petersson, H. Nakatsuji, X. Li, M. Caricato, A.V. Marenich, J. Bloino, B.G. Janesko, R. Gomperts, B. Mennucci, H. P. Hratchian, J.V. Ortiz, A.F., G09 | Gaussian.Com, Gaussian 16 (Gaussian, Inc., Wallingford CT, 2016). https://gaussian.com/citation_a03/, 2016 (accessed June 13, 2021).
[41] T. Lu, F. Chen, Multiwfn: A multifunctional wavefunction analyzer, J. Comput. Chem. 33 (2012) 580–592, https://doi.org/10.1002/jcc.22885.
[42] D. Hall, K. Stavrou, E. Duda, A. Danos, S. Bagnich, S. Warriner, A.M.Z. Slawin, D. Beljonne, A. Köhler, A. Monkman, Y. Olivier, E. Zysman-Colman, Diindolocarbazole – achieving multiresonant thermally activated delayed fluorescence without the need for acceptor units, Mater. Horiz. 9 (2022) 1068–1080, https://doi.org/10.1039/D1MH01383A.
[43] X. Gao, S. Bai, D. Fazzi, T. Niehaus, M. Barbatti, W. Thiel, Evaluation of spin-orbit couplings with linear-response time-dependent density functional methods, J. Chem. Theory. Comput. 13 (2017) 515–524, https://doi.org/10.1021/ACS.JCTC.6B00915.
[44] O.W. Morawski, P. Gawryś, A.L. Sobolewski, Harnessing proton-coupled electron transfer for hydrogenation of aza-arenes: photochemistry of quinoxaline derivatives in methanol, J. Phys. Chem. A 127 (2023) 8871–8881, https://doi.org/10.1021/ACS.JPCA.3C05077.
[45] H. Shi, W. Yao, W. Ye, H. Ma, W. Huang, Z. An, Ultralong organic phosphorescence: from material design to applications, Acc. Chem. Res. 55 (2022) 3445–3459, https://doi.org/10.1021/ACS.ACCOUNTS.2C00514.
[46] M. Yamazaki, Industrialization and application development of cyclo-olefin polymer, J. Mol. Catal. a Chem. 213 (2004) 81–87, https://doi.org/10.1016/J.MOLCATA.2003.10.058.
[47] Y. Kuwabara, H. Ogawa, H. Inada, N. Noma, Y. Shirota, Thermally stable multilared organic electroluminescent devices using novel starburst molecules, 4,4′,4″-tri(N-carbazolyl)triphenylamine (TCTA) and 4,4′,4″-tris(3-methylphenylphenylamino)triphenylamine (m-MTDATA), as hole-transport materials, Adv. Mater 6 (1994) 677–679, https://doi.org/10.1002/ADMA.19940060913.
[48] L. Marin, L. Lutsen, D. Vanderzande, W. Maes, Quinoxaline derivatives with broadened absorption patterns, Org. Biomol. Chem. 11 (2013) 5866, https://doi.org/10.1039/c3ob41059e.
[49] N.J. Hestand, F.C. Spano, Expanded theory of H- and J-molecular aggregates: the effects of vibronic coupling and intermolecular charge transfer, Chem. Rev. 118 (2018) 7069–7163, https://doi.org/10.1021/acs.chemrev.7b00581.
[50] Z. Zhou, X. Xie, Z. Sun, X. Wang, Z. An, W. Huang, Recent advances in metal-free phosphorescent materials for organic light-emitting diodes, J. Mater. Chem. C. Mater. 11 (2023) 3143–3161, https://doi.org/10.1039/D2TC05256C.
[51] S. Hirata, S. Hirata, Recent advances in materials with room-temperature phosphorescence: photophysics for triplet exciton stabilization, Adv. Opt. Mater. 5 (2017) 1700116, https://doi.org/10.1002/ADOM.201700116.
[52] M. Gmelch, T. Achenbach, A. Tomkeviciene, S. Reineke, High-speed and continuous-wave programmable luminescent tags based on exclusive room temperature phosphorescence (RTP), Adv. Sci. (Weinh) 8 (2021) e2102104, https://doi.org/10.1002/advs.202102104.
[53] Z. Yang, H. Liu, X. Zhang, Y. Lv, Z. Fu, S. Zhao, M. Liu, S.-T. Zhang, B. Yang, Photo-responsive dynamic organic room-temperature phosphorescence materials based on a functional unit combination strategy, Adv. Mater. 36 (2024) e2306784, https://doi.org/10.1002/adma.202306784.
[54] H.F. Higginbotham, M. Okazaki, P. de Silva, S. Minakata, Y. Takeda, P. Data, Heavy-atom-free room-temperature phosphorescent organic light-emitting diodes

enabled by excited states engineering, ACS. Appl. Mater. Interfaces. 13 (2021) 2899–2907, https://doi.org/10.1021/acsami.0c17295.
[55] M. Gao, P.L. Burn, A. Pivrikas, Balanced hole and electron transport in Ir(ppy) 3 : TCTA blends, ACS. Photonics. 8 (2021) 2425–2430, https://doi.org/10.1021/acsphotonics.1c00613.
[56] W.R. Laws, P.B. Contino, [21]Fluorescence quenching studies: analysis of nonlinear Stern-Volmer data, Methods Enzymol. (1992) 448–463, https://doi.org/10.1016/0076-6879(92)10023-7.
[57] R. Keruckiene, D. Volyniuk, K. Leitonas, J.V. Grazulevicius, Dual emission fluorescence/room-temperature phosphorescence of phenothiazine and benzotrifluoride derivatives and its application for optical sensing of oxygen, Sens. Actuators. B Chem. 321 (2020) 128533, https://doi.org/10.1016/j.snb.2020.128533.
[58] S. Wang, Z. Cheng, X. Han, H. Shu, X. Wu, H. Tong, L. Wang, Efficient and tunable purely organic room temperature phosphorescence films from selenium-containing emitters achieved by structural isomerism, J. Mater. Chem. C. Mater. 10 (2022) 5141–5146, https://doi.org/10.1039/D2TC00337F.